Efficiency of lamellipodia protrusion is determined by the extent of cytosolic actin assembly

Georgi Dimchev[a,b], Anika Steffen[b], Frieda Kage[a,b], Vanessa Dimchev[a,b], Julien Pernier[c], Marie-France Carlier[c], and Klemens Rottner[a,b,*]

[a]Division of Molecular Cell Biology, Zoological Institute, Technische Universität Braunschweig, 38106 Braunschweig, Germany; [b]Department of Cell Biology, Helmholtz Centre for Infection Research, 38124 Braunschweig, Germany; [c]Cytoskeleton Dynamics and Motility, Centre National de la Recherche Scientifique, 91198 Gif-sur-Yvette, France

ABSTRACT **Cell migration and cell–cell communication involve the protrusion of actin-rich cell surface projections such as lamellipodia and filopodia. Lamellipodia are networks of actin filaments generated and turned over by filament branching through the Arp2/3 complex. Inhibition of branching is commonly agreed to eliminate formation and maintenance of lamellipodial actin networks, but the regulation of nucleation or elongation of Arp2/3-independent filament populations within the network by, for example, formins or Ena/VASP family members and its influence on the effectiveness of protrusion have been unclear. Here we analyzed the effects of a set of distinct formin fragments and VASP on site-specific, lamellipodial versus cytosolic actin assembly and resulting consequences on protrusion. Surprisingly, expression of formin variants but not VASP reduced lamellipodial protrusion in B16-F1 cells, albeit to variable extents. The rates of actin network polymerization followed a similar trend. Unexpectedly, the degree of inhibition of both parameters depended on the extent of cytosolic but not lamellipodial actin assembly. Indeed, excess cytosolic actin assembly prevented actin monomer from rapid translocation to and efficient incorporation into lamellipodia. Thus, as opposed to sole regulation by actin polymerases operating at their tips, the protrusion efficiency of lamellipodia is determined by a finely tuned balance between lamellipodial and cytosolic actin assembly.**

Monitoring Editor
Paul Forscher
Yale University

Received: May 26, 2016
Revised: Feb 10, 2017
Accepted: Mar 17, 2017

INTRODUCTION

Actin polymerization can generate force, for example, through stochastic insertion of actin monomers onto the barbed ends of filament bundles or networks as found at the tips of lamellipodia and filopodia (Small *et al.*, 2002). Much progress has been made in recent years concerning description and analysis of essential regulators of actin filament assembly and disassembly in cell edge protrusions such as lamellipodia, including the branching activity of actin-related protein (Arp2/3) complex, its regulation in lamellipodia by suppressor of the cAMP receptor (Scar)/WASP-family verprolin-homologous (WAVE) complex, and regulation of the latter by ras-related C3 botulinum toxin substrate (Rac) subfamily GTPases (for reviews, see Campellone and Welch, 2010; Ridley, 2011; Steffen *et al.*, 2014). As opposed to actin turnover in the lamellipodium (Watanabe and Mitchison, 2002; Iwasa and Mullins, 2007; Lai *et al.*, 2008), the homeostasis of actin assembly and disassembly in the entire cell, including more-proximal, cytoplasmic regions, and its effect on protrusion has received little attention, although it has become increasingly clear that distinct subcellular actin domains can influence each other. This is illustrated by the apparent competition between actin structures formed by two main actin assembly factors, Arp2/3 complex and formins (Rotty *et al.*, 2015; Suarez *et al.*, 2015). In two dimensions, lamellipodia are flat networks of actin filaments, frequently associated with the substratum but capable as well of protruding while lifting upward and backward in a

This article was published online ahead of print in MBoC in Press (http://www.molbiolcell.org/cgi/doi/10.1091/mbc.E16-05-0334) on March 22, 2017.

*Address correspondence to: Klemens Rottner (k.rottner@tu-braunschweig.de).

Abbreviations used: Arp2/3, actin-related protein 2/3; Cdc42, cell division cycle 42; EGFP, enhanced green fluorescent protein; Ena/VASP, enabled/vasodilator-stimulated phosphoprotein; F-actin, filamentous actin; FMNL2, formin-like family member 2; FRAP, fluorescence recovery after photobleaching; PA, photoactivatable; Scar, suppressor of cAMP receptor; VASP, vasodilator-stimulated phosphoprotein; WAVE, WASP-family verprolin-homologous.

process termed ruffling. Lamellipodia protruding from apical cell surfaces or at the surface of round cells in three dimensions or in suspension are also called ruffles. Actin filament generation in lamellipodia, for example, through branching mediated by the Arp2/3 complex, is believed to occur at the interface of the actin network and plasma membrane (Wang, 1985; Iwasa and Mullins, 2007; Lai *et al.*, 2008) at sites enriched for various actin assembly factors, including the Arp2/3 activator WAVE and associated WAVE-complex subunits (Innocenti *et al.*, 2004; Steffen *et al.*, 2004), formins, such as formin-like family member 2 (FMNL2) and 3 (Block *et al.*, 2012; Kage *et al.*, 2017), and enabled/vasodilator-stimulated phosphoprotein (Ena/VASP) family members (Rottner *et al.*, 1999; Svitkina *et al.*, 2003). Arp2/3 complex and its continuous activation is considered essential for both initiation and maintenance of lamellipodial actin networks (Suraneni *et al.*, 2012; Wu *et al.*, 2012; Koestler *et al.*, 2013), but the contributions of each regulator to nucleation or elongation of actin filaments remains poorly defined. According to the dendritic nucleation model of branched actin network formation and turnover (Mullins *et al.*, 1998; Pollard and Borisy, 2003), filaments are generated and grow until capped, but relative filament numbers growing and pushing at any given time in the lamellipodium as compared with capped and/or depolymerizing filaments within the network are unknown. Similarly, the relevance of the ratio of actively growing filaments to nonproductive filaments within lamellipodia or elsewhere in the cell for protrusion efficiency has so far been unclear.

Additional outstanding questions include the precise extent of cooperation between different actin assembly factors within lamellipodia, in particular the Arp2/3 complex and Ena/VASP or formin-family polymerases. Formin family members have been proposed to operate both upstream—as generators of mother filaments for Arp2/3-dependent branching exemplified by mDia1 and 2 (Yang *et al.*, 2007; Isogai *et al.*, 2015)—and downstream or in parallel to Arp2/3 complex–dependent branching (Block *et al.*, 2012; Krause and Gautreau, 2014; Kage *et al.*, 2017). Of course, distinct formins or Ena/VASP family members could be endowed with various different functions, but we are just at the beginning of precisely dissecting the specific activities of all of these factors in lamellipodia relative to branching and/or filament capping.

Finally, protrusion efficiency also might be regulated by availability of actin monomer, although actin concentrations (Koestler *et al.*, 2009) and diffusion rates (McGrath *et al.*, 1998; Lai *et al.*, 2008) in vivo have appeared surprisingly high. Ideas for spatiotemporal control of actin monomers at sites of polymerization range from biased forward translocation (Zicha *et al.*, 2003) and cell edge accumulation (Vitriol *et al.*, 2013), as in a sink, to intralamellipodial recycling, on the possibility that short traveling distances could optimize the repolymerization of monomers after disassembly (Cramer, 1999; Vitriol *et al.*, 2015). Although not mutually exclusive, the respective relevance of each mechanism for optimal protrusion in different conditions and/or cell types is incompletely understood.

Here we used a straightforward gain-of-function approach in migrating B16-F1 melanoma cells and fibroblasts to explore effects of formin variant or VASP overexpression on various parameters of lamellipodium formation, including protrusion speed and rates of actin network polymerization, as well as Arp2/3 complex incorporation. To our surprise, we found little correlation between amount of lamellipodial actin filaments at any given time and protrusion efficiency, but we established the extent of cytosolic filamentous actin (F-actin) assembly as a prime determinant of effective lamellipodium protrusion.

RESULTS

Modulation of lamellipodium protrusion by overexpression of formin fragments or the Ena/VASP family member VASP

We previously found that knockdown of the FMNL formin subfamily member FMNL2 in B16-F1 cells reduces average protrusion rates of lamellipodia (Block *et al.*, 2012), which suggested that FMNL2-mediated actin assembly might promote protrusion rates of lamellipodial actin networks by accelerating actin network polymerization (Krause and Gautreau, 2014). We showed more recently that reduced protrusion upon FMNL2 or combined FMNL2 and 3 loss of function does not result from a decrease in rates of actin network polymerization but instead from significant filament loss and compromised force development of lamellipodial actin networks (Kage *et al.*, 2017). To test whether the rate of lamellipodium protrusion can at least be enhanced by experimentally increasing FMNL2 activity at the lamellipodium tip, we explored effects on protrusion by overexpression of full-length FMNL2 (isoform B; Block *et al.*, 2012) and a construct designated as FMNL2(8P)-C, which lacks regulatory domains dispensable for lamellipodial accumulation. Indeed, FMNL2 accumulation at lamellipodia tips required neither its N-terminal myristoylation nor an interaction with its regulatory GTPase cell division cycle 42 (Cdc42), consistent with previous data obtained using myristoylation-defective variants and/or Cdc42-deficient cells (Block *et al.*, 2012), but it was mediated in the case of FMNL2(8P)-C by the presence of sequences within the proline-rich FH1 and the actin-binding FH2 domain (for design of all constructs used in this study, see Figure 1A). More specifically, a detailed truncation analysis revealed that whereas the FH2 domain alone was insufficient for accumulation at the lamellipodium tip (Supplemental Figure S1A), the minimal construct allowing such a localization required both the FH2 domain and as few as 40 residues N-terminal to the FH2 domain (Supplemental Figure S1B). In contrast, neither full-length FMNL1 (unpublished data) nor FMNL1-FH1-FH2 (Figure 1B) localized to lamellipodia in B16-F1 cells. Hence, domain swap experiments between FMNL1 and 2 established that lamellipodial targeting of FMNL2 was a specific feature of its FH2 domain but also required the presence of proline-rich sequence stretches that could derive from either FMNL1 or FMNL2 (Supplemental Figure S1, C and D). Given that the domain swap variant harboring the FMNL1-FH2 completely failed to accumulate at the lamellipodium tip although it was readily expressed at its expected molecular weight (Supplemental Figure S1E), we concluded that actin binding alone in these formins mediated by each of their FH2 domains cannot explain the differences in localization between FMNL2(8P)-C and FMNL1-FH1-FH2, in particular because FMNL1 was previously established to potently assemble actin filaments (Harris *et al.*, 2006). Of interest, however, and in analogy to the differential behavior observed for FMNL1 and FMNL2 constructs in lamellipodia (Figure 1B), filopodia induction in Jurkat T-cells was also stimulated by FH1-FH2 of the FMNL2 relative FMNL3 but not of FMNL1 (Harris *et al.*, 2010). Apart from this, a fragment used here and encompassing the FH1 and FH2 domains of mDia1 also did not accumulate in lamellipodia (Figure 1, A and B). These observations provided a foundation for examining the effects exerted on lamellipodial dynamics either by enhanced green fluorescent protein (EGFP)–tagged formin variants capable of full regulation (FMNL2 full-length) compared with constitutively active constructs capable (FMNL2(8P)-C) or incapable (FMNL1-FH1-FH2 and mDia1-FH1-FH2) of accumulation at lamellipodia tips, or by the Ena/VASP family member VASP. Figure 1A summarizes a panel of constructs all capable in principle of actin assembly but displaying differential and only partially overlapping localizations (Figure 1B).

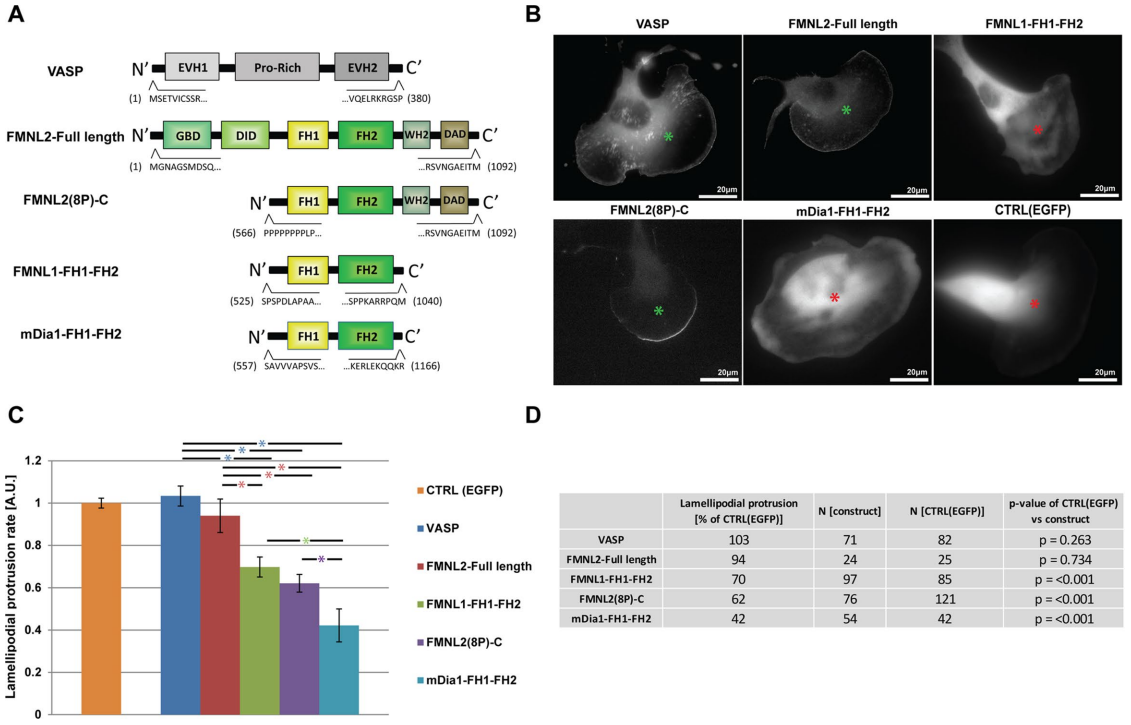

	Lamellipodial protrusion [% of CTRL(EGFP)]	N [construct]	N [CTRL(EGFP)]	p-value of CTRL(EGFP) vs construct
VASP	103	71	82	p = 0.263
FMNL2-Full length	94	24	25	p = 0.734
FMNL1-FH1-FH2	70	97	85	p = <0.001
FMNL2(8P)-C	62	76	121	p = <0.001
mDia1-FH1-FH2	42	54	42	p = <0.001

FIGURE 1: Rates of lamellipodium protrusion are differentially affected by overexpression of different actin-binding proteins. (A) The five constructs overexpressed in cells. The regulatory domains present in each construct, as well as the first (N-terminal) and last (C-terminal) amino acid residue positions are indicated. (B) Representative images of the subcellular localization of each construct expressed as EGFP-tagged version in migrating B16-F1 mouse melanoma cells. Green asterisks, lamellipodial localization; red asterisks, cytosolic localization. (C) Average lamellipodial protrusion rates of B16-F1 cells after overexpression of each of the five different constructs compared with EGFP-alone–expressing controls. Data are displayed as arbitrary units (A.U.) and arithmetic means ± SEM, as the value obtained for each construct was individually normalized and represented as fold change to its respective control (EGFP). The average protrusion speed of nonnormalized CTRL cells is 1.29 µm/min. (D) Average protrusion (as percentage of control), sample size (*N*) for each construct versus control, and *p* values from statistical comparisons of each construct with its individual control group by Mann–Whitney rank sum test.

The localization of both EGFP-tagged full-length FMNL2 and FMNL2(8P)-C was largely restricted to the lamellipodium tip, whereas VASP accumulated at the lamellipodium tip plus a rim of focal complexes or nascent adhesions shortly behind as well as in bona fide focal adhesions (Figure 1B), as expected (Rottner *et al.*, 1999; Svitkina *et al.*, 2003). In contrast, FMNL1-FH1-FH2 and mDia1-FH1-FH2 failed to accumulate at the lamellipodium tip, similarly to EGFP alone (Figure 1B), as confirmed by line-scan analysis (Supplemental Figure S2, A and B).

To our surprise, however, expression of none of these constructs increased lamellipodial protrusion rate significantly. Instead, all formin variants suppressed protrusion, albeit to various extents (Figure 1, C and D). Of interest, there was little correlation in B16 cells between the ability to accumulate at lamellipodia tips and the induced suppression of protrusion rate, as illustrated, for instance, by comparing the constructs corresponding to the FH1-FH2 domains of FMNL1 versus FMNL2. On average, suppression of protrusion was strongest on expression of mDia1-FH1-FH2 (down to 42% of EGFP-expressing controls), and no or at best very moderate suppression was observed on overexpression of VASP (103% of controls) and FMNL2 full-length (94% of controls), respectively. Of importance, plotting fluorescence of expressed constructs in individual cells against protrusion rate revealed that individual differences in expression level for each construct were by far less relevant than differences between distinct constructs. This is particularly evident when considering that a negative correlation between expression level and protrusion rate was statistically significant in the case of only one construct (FMNL1-FH1-FH2; Supplemental Figure S3). Moreover, expression levels of those constructs inhibiting protrusion most effectively—FMNL2(8P)-C and mDia1-FH1-FH2—were much less abundant than VASP, for example, at the other end of effectiveness, which was expressed far better, in spite of its modest effects (Supplemental Figure S3).

Thus, although overexpression of neither construct caused lamellipodia to disappear or to collapse in the process of protrusion (Supplemental Movie S1), as observed previously on sequestration, for example, of Arp2/3 complex by excess amounts of the C-terminus of Scar/WAVE (Machesky and Insall, 1998; Koestler *et al.*, 2013), none of the constructs used here was capable of stimulating actin assembly for promoting protrusion rates in this experimental setting. Thus not even those actin assembly factors capable of accumulating at the lamellipodium tip increased protrusion rates, but instead they suppressed or at best did not change them (VASP), which came as a surprise, given the correlations previously observed between protrusion rates and the amounts of endogenous FMNL formins present in cells (Block *et al.*, 2012) or of VASP at the lamellipodium tip (Rottner *et al.*, 1999). The fact that FMNL1-FH1-FH2 and mDia1 FH1-FH2, which fail to accumulate at the lamellipodium tip (Figure 1B), reduced protrusion at least as effectively as formin variants capable of accumulating there suggested that suppression

A

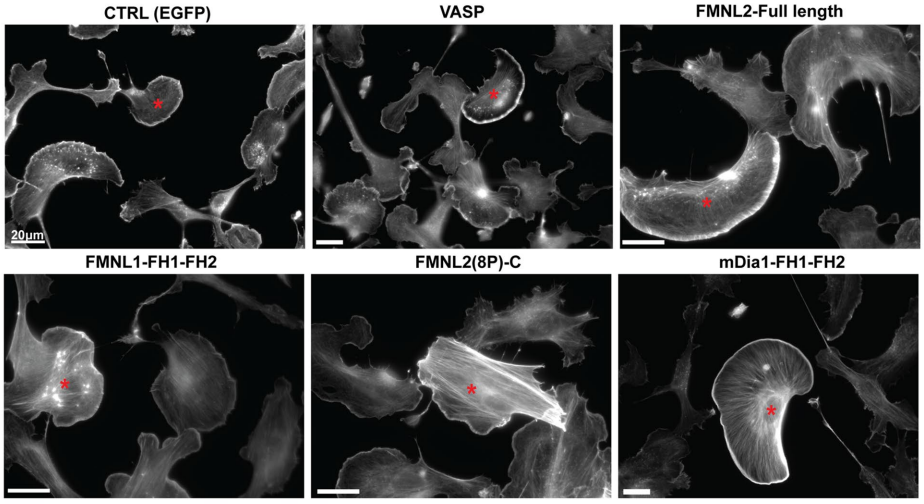

B

	EGFP (+) cells lam/cyto F-actin	Lamellipodial F-actin EGFP (+) / EGFP (-)	Cytosolic F-actin EGFP (+) / EGFP (-)	N
CTRL (EGFP)	1.66	1.01	1.03	49
VASP	2.51	2.27	1.29	58
FMNL2-Full length	2.16	2.21	1.54	122
FMNL1-FH1-FH2	1.37	2.17	2.07	88
FMNL2(8P)-C	1.59	2.27	2.09	51
mDia1-FH1-FH2	1.01	2.07	2.90	45

C

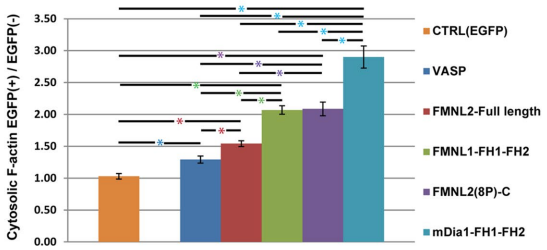

D

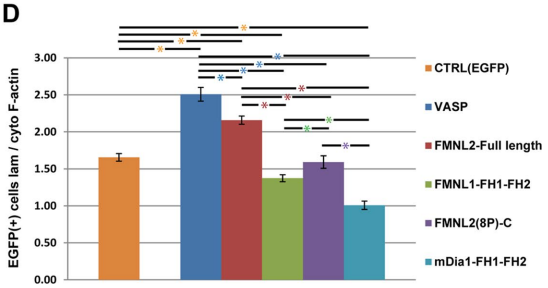

FIGURE 2: Effects of VASP or formin construct overexpression on lamellipodial and cytosolic F-actin distributions in B16-F1 cells. (A) Representative images of B16-F1 cells transfected with various constructs and stained for F-actin with phalloidin. Note increased F-actin staining in cells ectopically expressing the respective EGFP-tagged construct (red asterisks). (B) Average values of different F-actin intensity ratios for each of the five overexpressed constructs and control (pEGFP-C1). (C) Ratios of average cytosolic F-actin intensities of EGFP-positive to EGFP-negative cells within the same microscopic field of view for each indicated construct. (D) Average ratios of lamellipodial to cytosolic F-actin intensities in EGFP-positive cells expressing each construct. Data in C and D are arithmetic means ± SEM.

of protrusion by all these formin variants does not occur through their action at this site.

Formin variants and VASP distinctly affect actin filament generation in cytoplasm versus lamellipodium

To shed light on the mechanistic reasons for aforementioned observations, we explored the extent of actin filament generation by distinct constructs in both lamellipodium and cytoplasm.

Initially, F-actin staining using phalloidin was performed on cells overexpressing EGFP-tagged versions of each construct (Figure 2A) and lamellipodial F-actin intensities measured in EGFP-positive compared with EGFP-negative cells (nonexpressors) within the same microscopic field of view as controls. The ratios obtained between lamellipodial F-actin intensities in EGFP-positive versus EGFP-negative cells indicated that lamellipodial actin filament mass increased on average by more than two times after overexpression of any one of the five constructs but not on overexpression of EGFP alone as control (Figure 2B, column 3). However, no significant differences of lamellipodial F-actin intensities were observed on overexpression between the five experimental constructs (Figure 2B), irrespective of whether they were capable of localizing to lamellipodial tips or not (Figure 1B, Supplemental Figure S2, A and B). Thus differential generation of lamellipodial F-actin by distinct constructs could not account for the differences in protrusion rates observed (Figure 1, C and D).

Next we investigated the specificity of lamellipodial actin accumulation in each experimental scenario. We considered two parameters: 1) cytosolic F-actin amounts in cells overexpressing each given construct (EGFP(+) cells) compared with nonexpressing neighbors within the same microscopic field of view (EGFP(–) cells; Figure 2, B and C), and 2) the ratio of lamellipodial to cytosolic F-actin in construct overexpressing cells (EGFP(+) cells; Figure 2, B

and D). This analysis revealed that overexpression of both VASP and FMNL2 full-length induced more F-actin accumulation in lamellipodia relative to the cytosol than overexpression of the remaining formin fragments used. This indicates that the truncated FH1-FH2 constructs lacking important regulatory features present in full-length molecules likely trigger nonspecific F-actin accumulation, in particular in the cytosol. Moreover, the ratio of lamellipodial to cytosolic F-actin was significantly higher in VASP and FMNL2 full-length expressors than EGFP-alone–expressing controls (1.66) and significantly lower than the latter in cells overexpressing mDia1-FH1-FH2 (1.01). Ratios of lamellipodial to cytosolic F-actin in cells overexpressing FMNL1-FH1-FH2 and FMNL2(8P)-C were roughly in between (Figure 2B, column 2). Of interest, comparison of cellular F-actin intensities with the results from lamellipodial protrusion rates (Figure 1, C and D) revealed a positive correlation between the specificity of lamellipodial F-actin accumulation relative to the cytosol and lamellipodial protrusion rate, as well as a negative correlation between induced cytosolic F-actin levels and lamellipodial protrusion rates. For instance, mDia1-FH1-FH2 overexpression induced a nearly threefold (2.9) increase of cytosolic F-actin levels compared with EGFP-expressing control cells (1.03; Figure 2B, column 4) and caused the most dramatic reduction in lamellipodial protrusion speed observed with the panel of constructs used here (Figure 1, C and D). In contrast, cells overexpressing VASP displayed a much more moderate increase in cytosolic F-actin levels than nontransfected neighbors (1.29 times; Figure 2, B and C), which coincided with the absence of a significant change in protrusion rate (Figure 1, C and D).

Again, the amount of individual expressed construct was less relevant than the type of construct used because the majority of constructs did not display a statistically significant positive correlation between expression levels (expressed as fold fluorescence over background) and induction of cytosolic F-actin (Supplemental Figure S4).

Together these data suggested that instead of absolute changes of F-actin levels within the lamellipodium, both the ratio of induction in lamellipodium over cytosol and the total amount of F-actin induced in the cytosol appeared decisive for the effectiveness of protrusion. Moreover, the highest ratio of lamellipodial over cytosolic F-actin assembly, induced by VASP overexpression, eliminated adverse effects on protrusion in B16-F1 cells but was unable to significantly increase protrusion over control rates (103%; Figure 1), indicating that 1) induction of F-actin assembly by actin-binding proteins in these cells and experimental conditions (2.27 times in lamellipodia of VASP-overexpressing cells; Figure 2B) can be clearly uncoupled from protrusion efficiency, and, in more general terms, 2) protrusion efficiency in these cells plateaus at a level independent of expression of an individual protrusion regulator such as VASP.

Finally, observed changes in relative F-actin intensities were independent of overall changes in actin expression for most experimental conditions, except for FMNL2(8P)-C and mDia1-FH1-FH2, which increased actin expression moderately but statistically significantly by ~25% (Supplemental Figure S5). It is intuitive to assume that this was mediated by serum response factor–stimulated gene transcription being switched on in conditions of decreased actin monomer concentrations upon increased cytosolic F-actin (Rajakyla and Vartiainen, 2014), which, if correct, might have slightly alleviated effects obtained with these constructs and indeed constituted the first hint that the strong effects observed with these constructs may be caused by reduction of cytosolic actin monomer concentrations (see later discussion).

Experimentally induced suppression of protrusion correlates with reduced rates of actin network polymerization

Next we sought to determine the mechanistic reasons for the reduced rates of protrusion observed on overexpression of formin fragments. Reduced protrusion could be caused in theory by reduced rates of actin network polymerization but also by increase of rearward flow with unchanged levels of actin network polymerization, as observed for FMNL2/3 knockdown or knockout (Kage *et al.*, 2017), or by both. However, the evident negative correlation between extent of protrusion reduction and stimulated amount of cytosolic actin filaments (Figure 2B) led us to hypothesize that reduction of protrusion might reflect direct changes in lamellipodial actin network polymerization.

Rates of actin network polymerization can be determined in principle by fluorescence recovery of photobleaching (FRAP) of expressed EGFP-tagged actin (Lai *et al.*, 2008) or tracking of fluorescence inhomogeneities (speckle-like structures) in lamellipodia of cells expressing EGFP-tagged Lifeact (Riedl *et al.*, 2008), as illustrated in Supplemental Movie S2. Indeed, actin network polymerization rates of B16-F1 wild-type lamellipodia were virtually identical when determined by both methods (Kage *et al.*, 2017). However, because overexpression of EGFP-tagged β-actin increased protrusion rates (Kage *et al.*, 2017), in accordance with previously published data (Peckham *et al.*, 2001), we chose to analyze Lifeact speckle flow here.

We tracked fluorescent Lifeact speckles in cells co-overexpressing fluorescently tagged VASP, FMNL2 full-length, or truncated formin versions as before (Figure 1A). Formin constructs were routinely used as mCherry-tagged versions in these experiments and thus combined with EGFP-Lifeact, except for full-length FMNL2, which could only be discerned at the lamellipodium tip as an EGFP-tagged version, combined then with mCherry-tagged Lifeact. Control experiments revealed that FMNL2(8P)-C suppressed protrusion irrespective of the type of fluorescent tag used (Supplemental Figure S6), and cells overexpressing EGFP- or mCherry-tagged Lifeact had identical rates of protrusion (Supplemental Figure S7A) and actin network polymerization (Supplemental Figure S7B).

The determined rates of Lifeact speckle translocation showed that overexpressed actin assembly factors suppressed relative actin polymerization rates in lamellipodia in a manner highly similar to the suppression of protrusion (Figure 3, A and B). One difference was that rates of lamellipodial actin network polymerization seemed modestly decreased, as opposed to the protrusion rates observed on overexpression of VASP and FMNL2 full-length, which were largely unchanged (Figure 1, C and D). However, this difference was rather small and not statistically significant (Figure 3B).

Live-cell imaging of fluorescently tagged Lifeact in these experiments also enabled determination of lamellipodium width in each experimental condition (Figure 3C), which was again gradually suppressed, depending on expressed actin assembly construct and nicely following the pattern of effects on protrusion (compare with Figure 1, C and D). Of interest, plotting lamellipodial protrusion rates against widths of lamellipodia formed in all of these experimental scenarios revealed a clear correlation between these two parameters, with a statistically significant Spearman rank order r of 0.83 ($p \leq 0.0001$), confirming that rapid actin assembly and thus protrusion increase the size of the respective actin structure—in this case, the lamellipodium—at least when assuming actin disassembly pathways in these conditions to remain constant (Figure 3E). The robust correlation between protrusion rate and lamellipodium width was of course independent of construct overexpression, as can be seen from r values obtained for data sets after individual construct

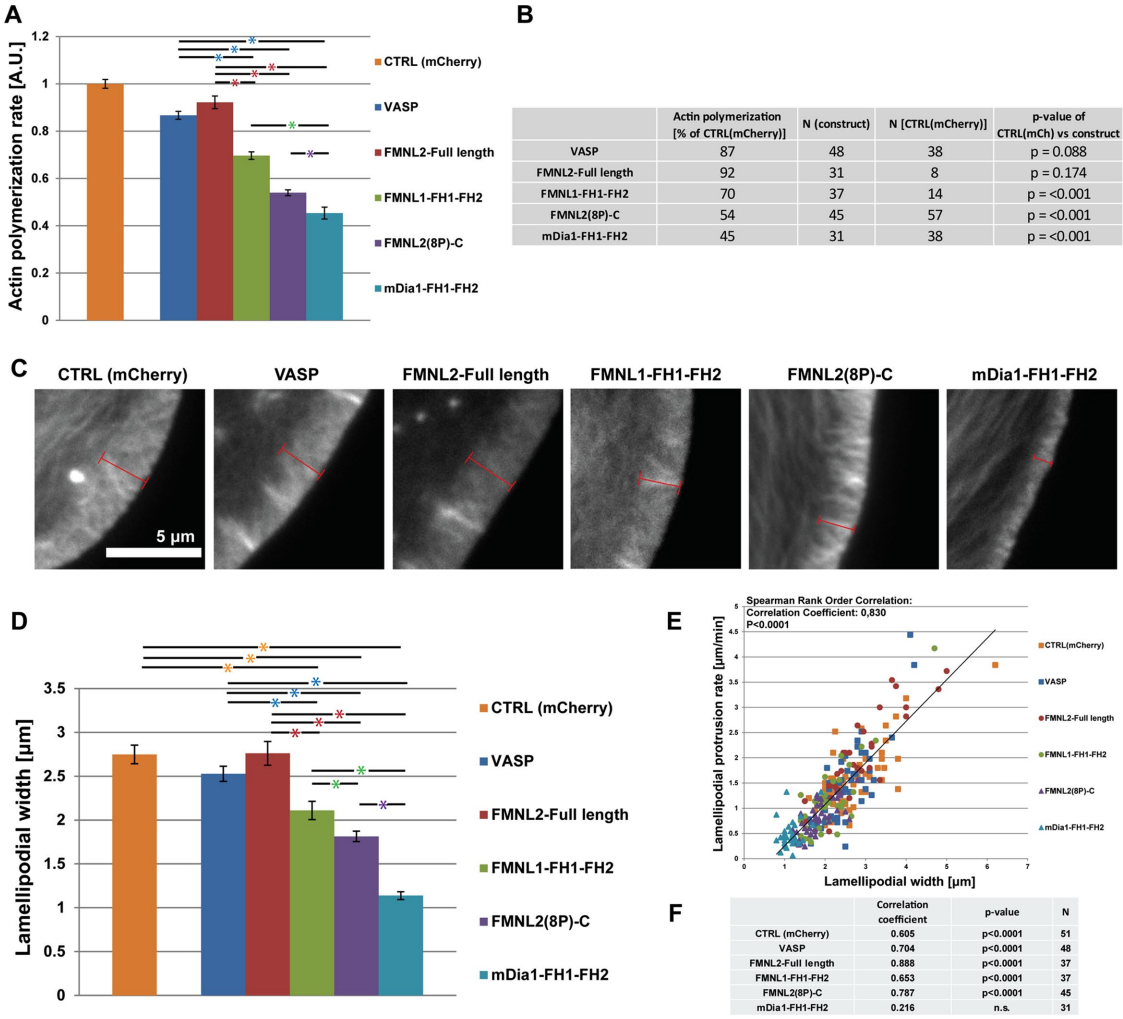

	Actin polymerization [% of CTRL(mCherry)]	N (construct)	N [CTRL(mCherry)]	p-value of CTRL(mCh) vs construct
VASP	87	48	38	p = 0.088
FMNL2-Full length	92	31	8	p = 0.174
FMNL1-FH1-FH2	70	37	14	p = <0.001
FMNL2(8P)-C	54	45	57	p = <0.001
mDia1-FH1-FH2	45	31	38	p = <0.001

	Correlation coefficient	p-value	N
CTRL (mCherry)	0.605	p<0.0001	51
VASP	0.704	p<0.0001	48
FMNL2-Full length	0.888	p<0.0001	37
FMNL1-FH1-FH2	0.653	p<0.0001	37
FMNL2(8P)-C	0.787	p<0.0001	45
mDia1-FH1-FH2	0.216	n.s.	31

FIGURE 3: Effects on actin polymerization rate and lamellipodium width on VASP and formin variant overexpression. (A) Average actin polymerization rates in cells overexpressing the constructs. Data are displayed as arbitrary units (A.U.) and arithmetic means ± SEM, as the value obtained for each construct was individually normalized and represented as fold change to its respective control (mCherry, except for FMNL2 full-length, which was used as EGFP-tagged variant and compared and normalized to cells overexpressing EGFP control). The average actin polymerization rate of nonnormalized CTRL cells is 4.02 µm/min. (B) Average rate of actin network polymerization (as percentage of control [CTRL]), sample size (*N*) for each construct vs. that of control (mCherry in all experiments, except for EGFP in the case of comparison with FMNL2 full-length; see description of A), and *p* values from statistical comparisons of each construct with its individual control group by Mann–Whitney rank sum test. (C) Representative Lifeact images derived from time-lapse movies of B16-F1 cells after co-overexpression of EGFP-tagged Lifeact with mCherry-tagged constructs or mCherry alone as control (CTRL; except for swapped fluorescent proteins in the case of FMNL2-full length, as before). Red line marks respective dimension of the lamellipodium. (D) Average values of lamellipodial width measured in live B16-F1 cells after co-overexpression of fluorescent protein–tagged Lifeact as before, with each of the five constructs and control. (E) Correlation analysis of lamellipodial protrusion rate vs. lamellipodial width indicates a statistically significant positive correlation between the parameters. For statistical analysis, values from all overexpressing constructs were combined and color-coded as indicated on the right. (F) Correlation coefficients (*r*) and *p* values from Spearman rank order correlation tests, as well as number of data points (*N*) for each individual construct.

overexpression (Figure 3F and Supplemental Figure S8). Moreover, the correlation was equally evident in cells overexpressing just mCherry as control. The only exception is that the correlation was not statistically significant for mDia1-FH1-FH2 (Supplemental Figure S8), the reason for which is unclear but should not be overrated because both parameters were comparably small and thus increasingly difficult to measure precisely on mDia1-FH1-FH2 overexpression.

Taken together, our data indicate a clear relationship between the spatial distribution and accumulation of cellular F-actin, lamellipodial actin polymerization rate, protrusion rate, and width. We propose that the disturbed balance of actin accumulating in cytosol versus lamellipodium can cause a reduction in filament polymerization rates at the lamellipodium tip, leading to reduced filament lengths, subsequent reduction of lamellipodial width, and protrusion.

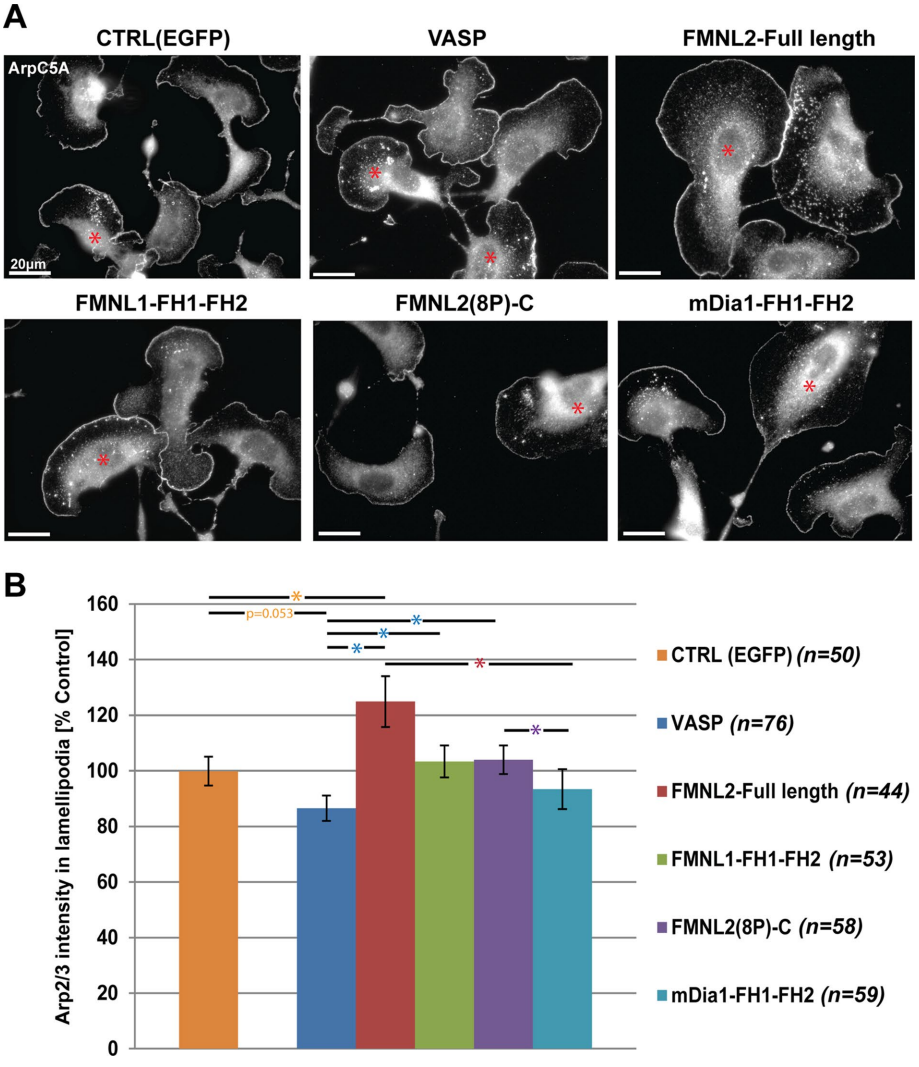

FIGURE 4: Quantification of Arp2/3 complex intensities in lamellipodia of B16-F1 cells overexpressing VASP and various formin fragments. (A) Representative images of B16-F1 cells immunostained for the Arp2/3 complex subunit p16A (ArpC5A) after overexpression of each of the five EGFP-tagged constructs or EGFP alone (CTRL). (B) Average intensity values of the Arp2/3 complex subunit p16A in lamellipodia of B16-F1 cells in experimental conditions as before and expressed as percentage of Arp2/3 intensity of EGFP-negative (i.e., nontransfected) cells within the same respective microscopic field of view for each cell. Data are arithmetic means ± SEM.

Of interest, cells expressing our panel of constructs had lamellipodial Arp2/3 complex intensities distinct from the pattern of F-actin increase in lamellipodia (Figure 4). More specifically, Arp2/3 complex intensities were virtually identical in control cells and those overexpressing FMNL1-FH1-FH2, FMNL2(8P)-C, and mDia1-FH1-FH2, indicating that Arp2/3-dependent branching was completely uncoupled from the increase of actin filaments caused by expression of these constructs in lamellipodia and cytosol (Figure 2B). In the case of FMNL2 full-length, we observed a slight increase in Arp2/3 complex intensity (~20%; Figure 4B), which might suggest that a fraction of the FMNL2 full-length–generated filaments serve as mother filaments for Arp2/3-mediated branching at the lamellipodium tip. This scenario would be consistent with the accumulation of FMNL2 at lamellipodia tips (Figure 1B) and the notion that Arp2/3 complex is incorporated at these sites (Miyoshi *et al.*, 2006; Iwasa and Mullins, 2007; Lai *et al.*, 2008). The lack of this effect observed with truncated FMNL2(8P)-C might suggest the requirement for additional regulatory domains flanking FH1-FH2 to coordinate FMNL2-induced filament generation with Arp2/3-dependent branching. If this is correct, however, such a function cannot be restricted to FMNL2 and/or its close FMNL family member FMNL3 also expressed in B16-F1 cells, as knockdown or knockout of both did not significantly reduce Arp2/3 complex staining of lamellipodia in spite of significant loss of average filament mass (Kage *et al.*, 2017). As opposed to FMNL2, VASP overexpression clearly decreased Arp2/3 complex intensities though not in a statistically significant manner (Figure 4B), consistent with the observation that Ena/VASP family members can increase the branch spacing of filaments in Arp2/3-dependent actin tails in vitro (Samarin *et al.*, 2003; Pernier *et al.*, 2016). Notwithstanding all this, we conclude that overexpression of the panel of actin-binding proteins used here had differential effects on protrusion and rates of lamellipodial actin network polymerization that were mostly uncoupled from Arp2/3 complex activation and integration.

Arp2/3 complex accumulation is largely uncoupled from lamellipodial actin filament generation by formin fragment overexpression

Expression of the panel of actin-binding proteins used here induced a strong, more-than-twofold increase of lamellipodial actin filament levels in B16-F1 cells (Figure 2), with variable effects on rates of lamellipodial protrusion and actin network polymerization (see earlier discussion). Lamellipodial actin filament networks are well established as requiring the branching activity of the Arp2/3 complex (Suraneni *et al.*, 2012; Wu *et al.*, 2012). To examine whether the stimulated increase of lamellipodial F-actin generation correlated with or was independent of Arp2/3 complex incorporation, we quantified endogenous Arp2/3 complex intensity on being stained with an antibody specific for ArpC5A (Millard *et al.*, 2003), which readily labeled protruding lamellipodia in these migrating cells (Block *et al.*, 2012).

Excess cytosolic actin polymerization coincides with capture in the cytosol and delayed translocation of actin monomers to the leading edge

We previously used bleaching of EGFP-tagged actin in the cytosol to directly visualize the rapid translocation of actin monomers to the protruding front, which was estimated to occur with a diffusion coefficient of ~5.5 µm^2/s (McGrath *et al.*, 1998; Lai *et al.*, 2008). More recently, we and others (Vitriol *et al.*, 2015) routinely used activation of photoactivatable (PA)-GFP-actin in the cytosol to directly visualize the translocation to and continuous incorporation of PA-GFP-actin

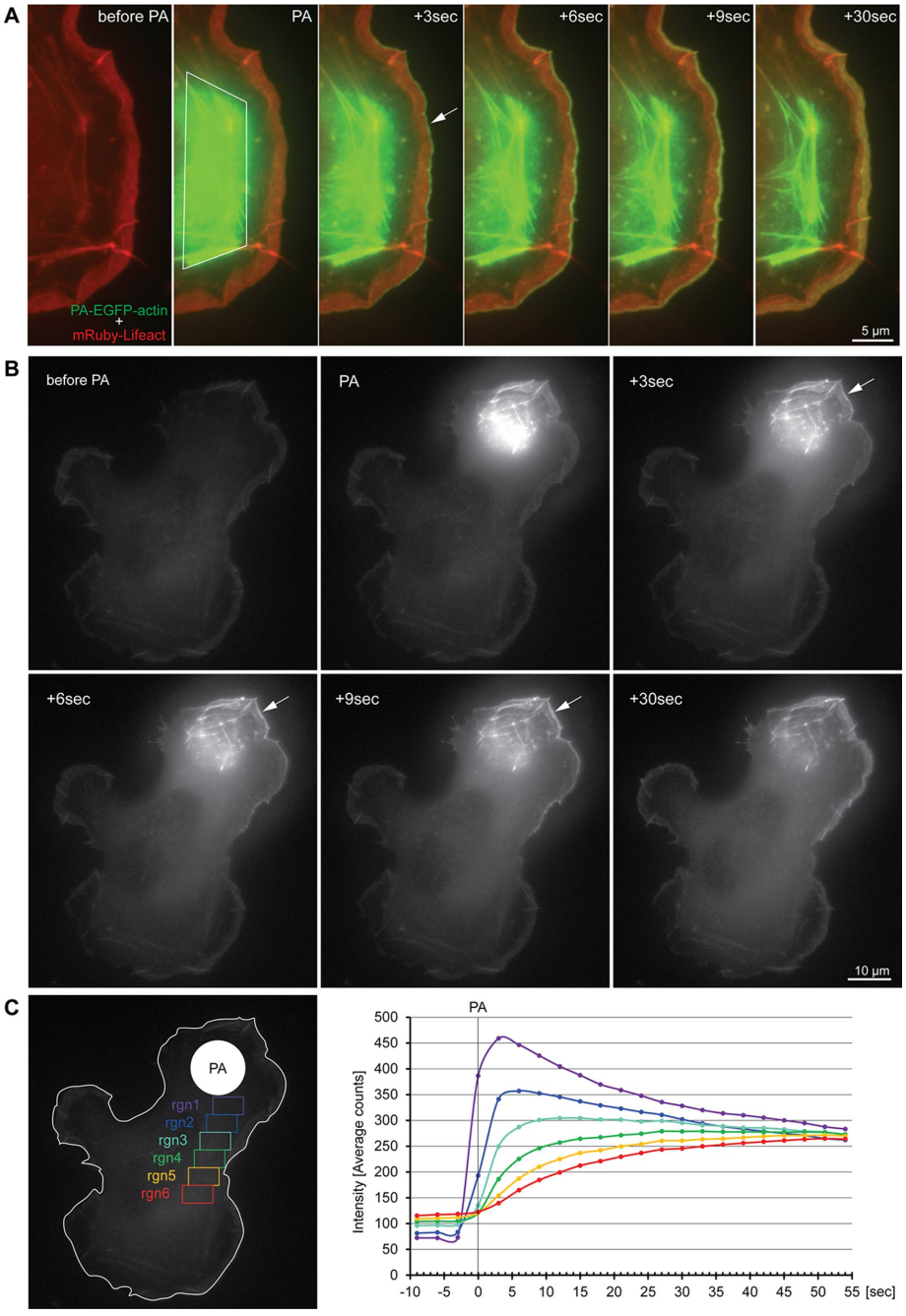

FIGURE 5: Analysis of actin diffusion and transport using photoactivation of PA-GFP-actin. (A) Migrating B16-F1 melanoma cell coexpressing mRuby-Lifeact (red) to visualize the actin cytoskeleton and PA-GFP-actin (green) to visualize translocation to and incorporation of actin monomers at the lamellipodium tip. PA, time point of photoactivation (0 s); the region of activation is marked with a white polygon at the time of activation. Note the rapid incorporation of PA-GFP-actin at the lamellipodium tip membrane (white arrow) soon after activation, as expected (Lai *et al.*, 2008; Vitriol *et al.*, 2015). (B) B16-F1 cell as in A, but displaying the PA-GFP-channel only, to illustrate the mobility of PA-GFP-actin throughout the cytosol of the photoactivated cell. Aside from incorporation of PA-GFP-actin into the lamellipodium (white arrows), rapidly moving photoactivated GFP-actin also illuminates the lamellipodium distal to the activation spot and the proximal cytoplasm as time after activation is progressing. (C) Fluorescence intensities measured as illustrated on the left vs. time after activation in distinct, color-coded cytosolic regions. Note the gradual reduction of average intensities with distance from the activation spot soon after activation (e.g., 5–10 s after activation) and the convergence of average fluorescence intensities, presumably due to cytoplasmic mixing by the end of the measurement (55 s).

at the lamellipodium tip (white arrow in Figure 5A). Note that incorporation from the lamellipodium tip is continuous because this treatment cannot distinguish whether actin resides as monomer or filament within the area of activation, and so incorporation over time first constitutes actin initially activated as monomer, followed by actin originally activated as filament and then continuously depolymerizing over time. The merged images show lamellipodium and proximal lamella of a migrating B16-F1 melanoma cell before and after activation of PA-GFP-actin. Coexpression of Ruby-tagged Lifeact in this case allowed following actin cytoskeleton dynamics before and after activation of PA-GFP-actin (red; see also Supplemental Movie S4). Aside from documenting the incorporation of PA-GFP-actin into the lamellipodium, we extended this approach to analyzing the mobility of PA-GFP-actin on activation within the cytoplasm, which is possible by combining photomanipulation with fast wide-field imaging (see *Materials and Methods*).

Again, photoactivation of PA-GFP-tagged actin over a short time period (<1 s; see *Materials and Methods*) in a region close to the lamellipodium generates an instantaneous flush of monomeric actin composed of both activated monomers diffusing through the region during activation and monomers depolymerizing from activated filaments within the same region. In the example shown, rapid highlighting of the lamellipodium close to the activation region by this monomer flush is followed by slower incorporation of activated monomers into the network (Figure 5B, arrows, and Supplemental Movie S5). However, the nondirectional flush of monomeric actin also causes its continuous propagation through the cytoplasm, roughly opposite to the direction of protrusion in this case (Figure 5, B and C). This type of nondirectional movement is of course independent of the activation site, and hence occurs in a manner indistinguishable at leading and trailing edges of the cell (unpublished data). Of interest, the observed "wave" of actin monomer was also delayed in time with increased distance of analyzed regions from the spot of activation and markedly reduced in intensity, presumably caused by continuously increased cytoplasmic mixing (Fakhri *et al.*, 2014) and thus dilution of photoactivated actin monomers (Figure 5C and Supplemental Movie S5).

The ability to directly visualize this type of actin transport made it possible to ask

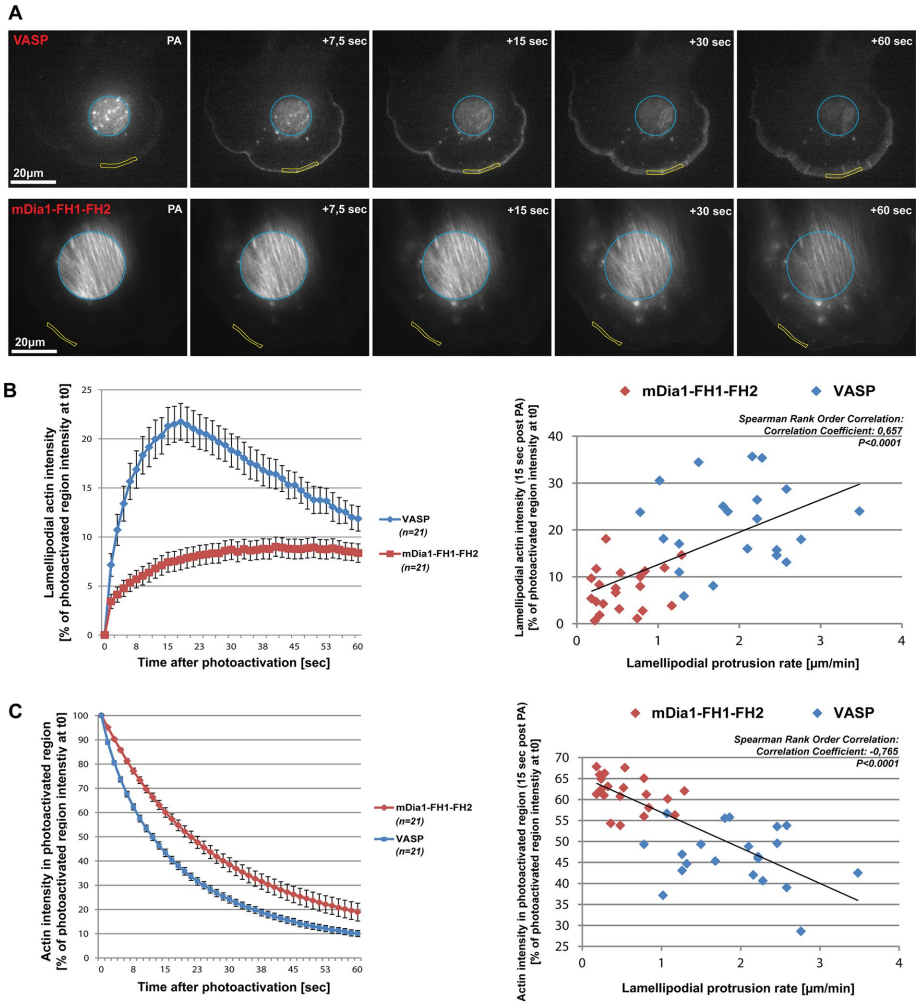

FIGURE 6: Differential translocation of PA-GFP-actin from cytosol to lamellipodium in B16-F1 cells overexpressing VASP vs. mDia1-FH1-FH2. (A) Representative images of B16-F1 cells overexpressing PA-GFP-actin and mCherry-tagged versions of either VASP or mDia1-FH1-FH2, with cytosolic regions photoactivated at time 0 (PA). Consecutive time-lapse frames recorded for the two experimental conditions showing subcellular kinetics of photoactivated GFP-actin over a time of 60 s. Regions of interest are as follows: region of photoactivation, turquoise; lamellipodial region measured (see later description) as specified in *Materials and Methods*, yellow. (B) Average fluorescence intensities of PA-GFP-actin in lamellipodial regions as exemplified in A (yellow area) and provided as percentage of intensities in respective photoactivation regions at time 0 (left). Experimental conditions are color-coded as indicated, and data are arithmetic means ± SEM. Note the lack of peak PA-GFP-actin incorporation in cells overexpressing mDia1-FH1-FH2 15–20 s after activation. The observed peak in cells overexpressing VASP (left) corresponds well with the positive correlation between protrusion rate and lamellipodial PA-GFP-actin intensity 15 s after activation (right; statistical significance confirmed by Spearman rank order correlation). On average, the shortest distance between lamellipodium tip and photoactivated region was 8.52 ± 2.18 µm for mDia1-FH1-FH2 and 8.41 ± 1.87 µm for VASP. (C) Left, analysis of dispersal of cytosolically photoactivated PA-GFP-actin from the activation spot in VASP- and mDia1-FH1-FH2–overexpressing B16-F1 cells. Right, correlation analysis as before, between dispersion of cytosolically photoactivated PA-GFP-actin from activation region at 15 s postactivation and lamellipodial protrusion rate. For correlation analyses in B and C, values from cells overexpressing VASP and mDia1-FH1-FH2 constructs were combined and color-coded as indicated. Area of the photoactivated region was 189 ± 60 µm^2 for mDia1-FH1-FH2 overexpressors and 127 ± 23 µm^2 for VASP overexpressors.

whether the decrease observed in rates of lamellipodial actin polymerization and protrusion on expression of the actin-binding proteins used here coincided not only with decreased incorporation, as would be expected if actin assembly is reduced, but also with reduced cytoplasmic actin mobility.

Figure 6 compares the fate of cytoplasmic actin in two extreme experimental scenarios—overexpression of VASP, which had little effect on rates of protrusion and lamellipodial actin network polymerization (see earlier discussion), and mDia1-FH1-FH2, which had the strongest effect on both parameters of lamellipodium protrusion.

We coexpressed PA-GFP-actin with an mCherry-tagged version of VASP or mDia1-FH1-FH2 (unpublished data) and photoactivated a region within the cytosol (Figure 6A). To explore the fate of the cytosolic pool of PA-GFP-actin, we initially measured 1) the average change in PA-GFP-actin intensity in the lamellipodium over time (Figure 6B) and 2) the loss of fluorescence in the photoactivated region over time (Figure 6C).

PA-GFP-actin incorporation allowed us to estimate the amount and speed of incorporation of cytosolically derived monomeric actin at lamellipodial tips during protrusion, which peaked at ~10–20 s on average after PA-GFP-actin activation in the cytosol of cells overexpressing mCherry-tagged VASP, followed by its continuous loss from the lamellipodium due to rapid turnover and distribution throughout the cell (Figure 6B, left). In contrast, incorporation of PA-GFP-actin at the tips of protruding lamellipodia was delayed and strongly reduced in intensity (relative to the intensity in the activation region) in cells overexpressing mDia1-FH1-FH2. In principle, reduced intensity of PA-GFP-actin at the lamellipodium tip could be caused simply by its delayed incorporation due to reduced rates of actin network polymerization in these conditions (Figure 3A), reduced translocation through the cytoplasm, or both. Indeed, we found a clear correlation between rates of lamellipodium protrusion and lamellipodial PA-GFP-actin incorporation (expressed as intensity relative to photoactivated region) 15 s after cytosolic PA-GFP-actin activation, which clearly depended on construct overexpression (Figure 6B, right). This indicated that reduced actin translocation to lamellipodia followed by reduced actin assembly at these sites directly translates into diminished protrusion in these experimental conditions, as expected (see earlier discussion).

However, to examine whether reduced incorporation at lamellipodia tips was preceded by decreased translocation of PA-GFP-actin throughout the cytosol, we also measured loss of fluorescence in the activation region in the case of VASP versus mDia1-FH1-FH2 overexpression. Of interest, average loss of fluorescence over time in the cytosolic activation region was strongly delayed on average in mDia1-FH1-FH2

overexpressors compared with the same cells expressing VASP. This analysis demonstrated that PA-GFP-actin is captured in the cytoplasm more efficiently in cells expressing mDia1-FH1-FH2, likely in the form of filaments, which are 2.25 times more abundant in these cells than in cells overexpressing VASP (Figure 2). Of most importance, a clear negative correlation was observed between extent of actin immobilization in the activation region 15 s postactivation and rate of lamellipodium protrusion (Figure 6C, right), showing that effects on protrusion can be deduced by the amount of actin remaining associated with the cytosolic compartments and suggesting that its delayed transport directly affects the efficiency of protrusion.

Note that in this set of experiments, activation regions in cells expressing mDia1-FH1-FH2 were chosen to be larger on average than in VASP-overexpressing cells to ensure that the strong reduction in actin incorporation in the lamellipodium (Figure 6B) is not caused by reduced generation of activated actin monomer. However, repeating these experiments with activation regions comparable in size and with all five overexpression constructs used here plus mCherry alone as control confirmed three important points. First, the differences observed between VASP and mDia1-FH1-FH2 in Figure 6 were largely independent of the activation region used (Supplemental Figure S9). Second, both kinetics of actin monomer incorporation at the lamellipodium tip and loss from the activation region followed a pattern that nicely correlated with actin-based protrusion and rates of actin network polymerization. Finally, both kinetic parameters of photoactivated actin were highly similar for cells overexpressing mCherry-tagged VASP or mCherry as control (Supplemental Figure S9). Average sizes and distances of activation regions to the lamellipodium tip for each construct are given in Supplemental Figure S9C.

Finally, we measured diffusion of PA-GFP-actin through cytosolic regions outside the spot of activation and at variable distances from it (Supplemental Figure S10, left). Consistently, VASP-overexpressing cells had a much higher mobility of PA-GFP-actin in cytoplasm than mDia1-FH1-FH2 overexpressors (Supplemental Figure S10, right). In regions close to the activation spot, PA-GFP-actin intensities were high at early time points after activation in VASP overexpressors but declined rapidly with time, whereas mDia-FH1-FH2 overexpressors displayed a much more homogeneous intensity of PA-GFP-actin during the time course after activation, with lower intensities than in VASP overexpressors at earlier time points after activation and higher intensities at later time points, likely because PA-GFP-actin was captured more efficiently in these cells. Of interest, in regions fairly distant from the activation region, PA-GFP-actin intensities in mDia1-FH1-FH2 overexpressors did not exceed those observed in VASP overexpressors, at least during the time course of analysis (Supplemental Figure S10, bottom right), indicating that, as opposed to a region close to the activation spot, actin monomer was less likely to reach those distantly located regions and incorporate into the actin structures at these sites before being distributed throughout the entire cell.

Collectively the data confirm reduced average diffusion and mobility of actin in cells overexpressing mDia1-FH1-FH2 compared with controls or to cells overexpressing VASP (Figure 6 and Supplemental Figure S9) and show clear correlations at the individual cell level between cytosolic actin mobility and effectiveness of protrusion, which strictly depended on actin network polymerization in these experiments. That reduced mobility in the cytosol directly affected the incorporation of PA-GFP-actin into the lamellipodium was confirmed again by correlation analysis (Supplemental Figure S11), as expected, strongly suggesting that excess cytosolic F-actin content generated by mDia1-FH1-FH2 overexpression captures and thus immobilizes actin monomer required at the cell periphery for effective protrusion.

Effects of formin construct and VASP overexpression in 3T3 fibroblasts

To confirm the general relevance of our results obtained in B16 cells, we performed a number of experiments in the commonly used and generally available cell line NIH-3T3. In these fibroblasts, overexpression of all constructs reduced rates of lamellipodial protrusion (Supplemental Figure S12A) and actin network polymerization (Supplemental Figure S12B) compared with EGFP-alone–overexpressing controls, with VASP being the least effective and mDia1-FH1-FH2 being the most effective of the panel of constructs (Figure 1A and Supplemental Figure S12), as observed in B16-F1 cells. Moreover, these effects correlated well with induction of actin polymerization in lamellipodium versus cytoplasm (Supplemental Figure S13, A and B). Consistent with observations in B16-F1 melanoma cells, we found clear induction of cytosolic actin filaments in particular with those constructs reducing protrusion most efficiently (Supplemental Figure S13). Induction of actin assembly in the lamellipodium by overexpression of each construct was generally less strong in NIH-3T3 fibroblasts than in B16-F1 cells (compare Figure 2B and Supplemental Figure S13B, column 3), and less homogeneous, but again, we found a reasonably consistent correlation between reduction of protrusion induced by each construct and reduction of the ratio of lamellipodial to cytoplasmic F-actin (Supplemental Figure S13D).

We thus conclude that effects on actin dynamics observed by the panel of overexpression constructs are largely conserved mechanistically between mouse melanoma and NIH-3T3 fibroblasts.

DISCUSSION

In this study, we used a gain-of-function approach to explore functional relationships between protrusion efficiency of the lamellipodium and extent of actin polymerization stimulated at these sites, as well as in ectopic cellular regions such as the cytoplasm. We were fortunate to find a set of constructs that affected protrusion and actin polymerization rate to a highly distinctive extent, making it possible for the first time to directly address the relevance of lamellipodial versus cytoplasmic actin assembly and specificity for the efficiency of lamellipodia protrusion. It had been commonly assumed that specific actin assembly factors such as Ena/VASP family members or formins (e.g., FMNL2) promote elongation of specific filaments within lamellipodia and thereby accelerate rates of lamellipodial protrusion (Krause and Gautreau, 2014). In this simplified but reasonably comprehensive scenario, protrusion rates would be balanced by two main activities: Arp2/3-dependent branching, which generates highly dense, stiff networks protruding slowly, and actin filament elongation by Ena/VASP family members and/or formins, promoting less branched, more loosely organized networks protruding rapidly. This hypothesis is consistent, for instance, with the previously observed linear dependence on protrusion rate of EGFP-VASP accumulation at the lamellipodium tip (Rottner *et al.*, 1999) and the observation of highly ruffling and labile lamellipodia in cells in which Ena/VASP family members were experimentally targeted to the plasma membrane through CAAX targeting (Bear *et al.*, 2000). Note, however, that Ena/VASP sequestration at the plasma membrane by CAAX targeting is not necessarily functionally equivalent to the simple tuning of Ena/VASP levels by loss-of-function approaches or overexpression of wild-type Ena/VASP protein (see later discussion). Moreover, loss of the formin FMNL2 reduced protrusion efficiency (Block *et al.*, 2012), but it was unclear whether this was indeed due to reduced rates of actin network polymerization

as proposed or to other reasons. Indeed, in a more recent, complementary study, we established that loss of FMNL2 and its close relative FMNL3 in migrating cells compromises protrusion and migration efficiency without affecting rates of lamellipodial actin network polymerization (Kage *et al.*, 2017). Moreover, none of the previous experiments assessed the direct effects of Ena/VASP family or formin overexpression on protrusion efficiency and other parameters of lamellipodia function, such as rates of actin network polymerization or lamellipodial Arp2/3 complex incorporation, as performed here.

Taking seriously the model of antagonizing activities of branching versus actin filament elongation promoting, respectively, stable and slow versus labile and fast protrusion, one would propose that shifting the balance of activities toward actin filament elongation by, for example, overexpressing actin filament elongators should decrease branching and increase protrusion rate. However, none of these assumptions turned out to be correct. In essence, the panel of overexpression constructs analyzed here uncovered three major surprises.

First, it appears to be impossible to increase protrusion efficiency by increasing levels of actin filament assembly factors, irrespective of whether these assembly factors harbor an intrinsic lamellipodial localization activity or are "designed" to accumulate at the lamellipodium tip. Instead, overexpression of full-length VASP or FMNL2 formin, as well as of various truncated formin variants, invariably increased lamellipodial F-actin content, at least in B16-F1 cells, without increasing rates of lamellipodial protrusion, which *by definition* depend on the rate of actin polymerization (Small *et al.*, 2002; Pollard and Borisy, 2003). In fibroblasts, induction of lamellipodial actin filaments appeared more stringently connected to the principal capability of localization of the respective construct to the lamellipodium tip (Figure 1B, Supplemental Figure S13B, and unpublished data), with reasons for the modest differences in this context between B16-F1 and fibroblasts being unclear. Of greater importance, however, and fully consistent in both cell types, none of the constructs was capable of increasing the speed of protrusion or of polymerization of the lamellipodial actin networks. Hence, in spite of VASP levels linearly accumulating with protrusion and thus actin polymerization rate and FMNL2 formin or FMNL2/3 double knockdown reducing the speed of lamellipodium protrusion (Block *et al.*, 2012; Kage *et al.*, 2017), increasing VASP or FMNL2 levels does not cause an increase of protrusion of respective lamellipodial networks. These data suggest that rates of lamellipodial protrusion and actin network polymerization are less directly controlled by and perhaps separable from the direct activities of actin assembly factors positioned at the interface between lamellipodium network and plasma membrane. It is likely, for instance, that increase of actin assembly factors at the lamellipodium tip increases actin nucleation and/or elongation at the tip, but this alone is not sufficient to increase the protrusion and rate of actin polymerization of the entire network. Such a scenario would also be consistent again with FMNL2/3 loss-of-function phenotypes, reflecting cells protruding more slowly and less efficiently due to their harboring reduced quantities of lamellipodial actin filaments and bundles in spite of unchanged rates of actin network polymerization (Kage *et al.*, 2017).

Second, all constructs examined in the context of B16-F1 lamellipodia had either no detectable effect on protrusion and lamellipodial actin network polymerization or decreased these parameters to variable extents. This was seen in spite of a significant but almost invariable increase, for the constructs used, of lamellipodial actin filament density (between 2.07- and 2.27-fold, depending on construct, and compared with lamellipodia of nontransfected cells). In fibroblasts, results were slightly more variable in extent, in particular concerning the induction of lamellipodial actin filaments by distinct constructs (see earlier discussion), but followed the same trend of reducing protrusion to an extent that depended on the construct used, with VASP being least and mDia-FH1-FH2 most effective. In both cell types, the amount of cytosolic actin filaments generated in the various overexpression conditions was much more relevant for protrusion than the extent of lamellipodial actin polymerization.

Third, in spite of previous data suggesting actin monomer concentrations in migrating B16-F1 melanoma cells to be in the 100 µM range, appearing incompatible with actin concentrations being rate limiting for assembly (Koestler *et al.*, 2009), we show here that conditions that favor excess cytosolic over lamellipodial actin assembly—for example, by overexpressing mDia1-FH1-FH2—delay actin monomer translocation to the cell periphery and coincide with actin monomer being captured in nonprotrusive, cytosolic compartments. We propose that this "nonproductive capture" is causative for the experimentally induced reduction of actin assembly-dependent protrusion at the cell periphery. In conclusion, the data presented here collectively suggest that productive protrusion requires the coordination of both lamellipodial actin assembly and cytosolic actin filament disassembly and that the availability of polymerizable actin monomer in cells determines rates of lamellipodial actin network polymerization rather than the biochemical activities of actin assembly factors residing at lamellipodia tips. The latter factors, exemplified by the activity of FMNL-subfamily formins, are crucial instead for actin assembly at the individual filament level, because their removal from lamellipodia reduced (Kage *et al.*, 2017) and their overexpression enhanced lamellipodial actin filament densities in a way that was separable from the effects of both treatments on protrusion.

MATERIALS AND METHODS

Cell culture, coverslips, and transfections

B16-F1 mouse melanoma cells (CRL-6323; American Type Culture Collection, Manassas, VA) were grown in DMEM and 4.5 g/l glucose (Life Technologies, Thermo Fisher Scientific, Germany) with 10% fetal calf serum (FCS; PAA Laboratories, Linz, Austria), 2 mM glutamine (Life Technologies), and 5000 U/ml penicillin-streptomycin (Life Technologies) at 37°C and 7% CO_2. NIH-3T3 mouse fibroblast cells were grown in DMEM and 4.5 g/l glucose (Life Technologies) supplemented with 10% FBS (054M3396; Sigma-Aldrich, Taufkirchen, Germany), 2 mM glutamine (Life Technologies), 1 mM sodium pyruvate (Life Technologies), 1% 100× Minimum Essential amino acids (Life Technologies), and 5000 U/ml penicillin-streptomycin (Life Technologies) at 37°C and 7% CO_2. Cells were transfected with 200 ng of vector DNA (as indicated) using JetPei (Polyplus Transfection, Illkirch, France) or peqFECT (PeqLab, VWR Life Science, Germany) transfection reagents.

B16-F1 cells were plated onto acid (HCl)-washed glass coverslips coated with 25 µg/ml laminin (L-2020; Sigma-Aldrich) in 50 mM Tris, pH 7.4, and 150 mM NaCl before fixation or videomicroscopy. The 12-mm-diameter coverslips were coated with 150 µl of laminin solution for 1 h, followed by washing with phosphate-buffered saline (PBS).

DNA constructs

pPUR vector mediating puromycin resistance for selection of transfected B16-F1 cells was purchased from Clontech (Mountain View, CA). EGFP-tagged, full-length VASP and mRFP-Ruby- or EGFP-tagged Lifeact, kindly provided by Roland Wedlich-Söldner (University of Münster, Münster, Germany) were described in

Carl *et al*. (1999) and Riedl *et al*. (2008), respectively. FMNL2-EGFP was prepared as follows: a DNA fragment of human FMNL2B protein (encompassing amino acid residues 1–1092) was amplified by PCR from cDNA and ligated into EGFP-N1 vector using the following forward and reverse primers containing *Nhe*I and *Sac*II restriction sites, respectively: 5′-GAGGCTAGCATGGGCAACGCAGGGAGC A-3′ (forward) and 5′-GAGACCGCGGCATTGTTATTTCGGCA-3′ (reverse). EGFP-tagged FMNL2(8P)-C insert was subcloned into an EGFP-C1 vector from an FMNL2(8P)-C construct encompassing amino acid residues 566–1092 of FMNL2-B (isoform 2) and described previously (Block *et al*., 2012), using the following forward and reverse primers containing *Sal*I and *Sac*II restriction sites, respectively: 5′-ATAGTCGACCCACCTCCCCCACCGCC-3′ (forward) and 5′-GCTCCGCGGTCACATTGTTATTTCGG-3′ (reverse).

For generation of EGFP-tagged FMNL1-FH1-FH2, a DNA fragment of human FMNL1 protein (encompassing amino acid residues 525–1040, which lacked the unstable, proline-rich region corresponding to residues 589–612) was amplified by PCR from cDNA using primers 5′-GAGGAATTCAGCCCTTCTCCTGATCTG-3′ (forward) and 5′-GAGGGATCCGGTCGCTCTCGTAGATCA -3′ (reverse) and ligated into EGFP-C2 vector with *Eco*RI and *Bam*HI restriction enzymes. For generation of mDia1-FH1-FH2, a DNA fragment encoding for amino acids 557–1166 of murine mDia1 but lacking the repetitive sequence corresponding to residues 667–679 was amplified and cloned into EGFP-C1 vector using the following forward and reverse primers containing *Bgl*II and *Sal*I restriction sites, respectively: 5′-GAGAGATCTGCTGTGGTTGTTGCACCTTC-3′ (forward) and 5′-GAGGTCGACCGCTTCTGCTGCTTCTCCAG-3′ (reverse).

Constructs used in Supplemental Figure S2 were generated as follows: for EGFP-FMNL2-FH2 construct, a DNA fragment of human FMNL2 isoform 2 (encompassing amino acid residues 616–1026) was amplified by PCR from cDNA using primers 5′-GAGAGTCGACATCAAAAAGCCCATC-3′ (forward) and 5′-GAGACCGCGGCTATTGCTGCTGCCTC-3′ (reverse) and ligated into EGFP-C1 vector with *Sal*I and *Sac*II restriction enzymes.

For the EGFP-FMNL2-L40aa-FH2 construct, a DNA fragment of human FMNL2 isoform 2 (encompassing amino acid residues 576–1026) was amplified by PCR from cDNA using primers 5′-GAGAGTCGACGGGCCCGCAGCTGAG-3′ (forward) and 5′-GAGACCGCGGCTATTGCTGCTGCCTC-3′ (reverse) and ligated into EGFP-C1 vector with *Sal*I and *Sac*II restriction enzymes.

For the EGFP-FMNL2-L40aa-FMNL1-FH2 construct, a DNA fragment of human FMNL2 isoform 2 (encompassing amino acid residues 576–615) was amplified by PCR from cDNA using primers 5′-GAGAGTCGACGGGCCCGCAGCTGAG-3′ (forward) and 5′-GATGGGCTTCTTGGCCTTCACGGCTGCCAGG-3′ (reverse). A DNA fragment of human FMNL1 isoform 1 (encompassing amino acid residues 632–1040) was amplified by PCR from cDNA using primers 5′-CCTGGCAGCCGTGAAGGCCAAGAAGCCCATC-3′ (forward) and 5′-GAGACCGCGGCTACATCTGTGGCCGTCTGGC-3′ (reverse). Both fragments were aligned by overlap extension PCR, and the resulting larger fragment was ligated into EGFP-C1 vector with *Sal*I and *Sac*II restriction enzymes.

For the EGFP-FMNL1-L40aa-FMNL2-FH2 construct, a DNA fragment of human FMNL1 isoform 1 (encompassing amino acid residues 592–631) was amplified by PCR from cDNA using primers 5′-GAGAGTCGACCCACCTCCACCTGGC-3′ (forward) and 5′-TGATGGGCTTTTTGATCTTCACGCCTGGTCCCA-3′ (reverse). A DNA fragment of human FMNL2 isoform 2 (encompassing amino acid residues 616–1026) was amplified by PCR from cDNA using primers 5′-TGGGACCAGGCGTGAAGATCAAAAAGCCCATCA-3′ (forward) and 5′-GAGACCGCGGCTATTGCTGCTGCCTC-3′ (reverse). Both fragments were aligned by overlap extension PCR, and the resulting larger fragment was ligated into EGFP-C1 vector with *Sal*I and *Sac*II restriction enzymes.

mCherry-tagged versions of the aforementioned constructs were generated by replacing EGFP in EGFP-C backbone vectors (Clontech) containing the respective inserts with mCherry using *Nhe*I and *Bsr*GI restriction enzymes.

mCherry-Lifeact was made by PCR-amplifying the cDNA sequence of mCherry (236 amino acid residues) using primers 5′-ACGGGATCCATTAAGCTTGCCACCATGG-3′ (forward) and 5′-CGTTATGCGGCCGCTTGTACAGCTCGTCC-3′ (reverse) containing *Bam*HI and *Not*I restriction sites, respectively, and replacing it for mRFPruby in Lifeact-EGFP-N1-mRFPruby vector (Riedl *et al*., 2008) using *Bam*HI and *Not*I restriction enzymes.

pEGFP-actin was purchased from Clontech, and PA-GFP-actin was as described (Koestler *et al*., 2008).

Immunofluorescence and phalloidin staining

For all fixations, solutions were prewarmed to 37°C. For staining, B16-F1 cells were washed with PBS, preextracted with 0.1% Triton X-100 in PBS for 1 min, and fixed with 4% paraformaldehyde in PBS for 20 min. For immunostaining, cells were blocked with 5% horse serum in 1% bovine serum albumin/PBS and then stained with antibodies and embedded into mounting medium following standard procedures.

Fluorescence intensities of lamellipodial components such as actin and p16A/ArpC5A (Clone 323H3; Olazabal *et al*., 2002) were determined by defining a region restricted to the lamellipodium and a larger, extracellular region (defined as background). Average pixel intensities in background regions were subtracted from average intensities in lamellipodial regions. Subtracted fluorescence intensities in lamellipodial regions of cells overexpressing various GFP-tagged constructs are presented as the percentage of the subtracted lamellipodial fluorescence intensities of GFP-negative cells within the same microscopic field of view. Obtained values from at least three independent experiments are averaged and represented as bar plots. Alexa Fluor 594–conjugated goat anti-mouse secondary antibody and Alexa Fluor 594–conjugated phalloidin were purchased from Invitrogen (now Thermo Fisher Scientific, Germany). For phalloidin staining, B16-F1 cells were transfected with constructs as indicated and fixed 2 d posttransfection, and F-actin intensity values were measured both in cytosol and lamellipodia with ImageJ software v1.46r (http://imagej.nih.gov/ij/).

Images of fluorescently labeled cells were generated essentially as described (Steffen *et al*., 2013) using 40×/1.3 numerical aperture (NA) Plan Apochromat, 63×/1.4 NA Plan Apochromat, or 63×/1.25 NA Plan Neofluor oil objectives.

Live-cell imaging (phase contrast and epifluorescence)

B16-F1 cells seeded on glass coverslips were observed in an open heating chamber (Warner Instruments, Hamden, CT) with a heater controller (TC-324 B, SN 1176) at 37°C. Cells were maintained in microscopy medium (Ham's F-12 4-(2-hydroxyethyl)-1-piperazineethanesulfonic acid–buffered medium; Sigma-Aldrich) including 10% FCS (PAA Laboratories), 2 mM glutamine, and 5000 U/ml penicillin-streptomycin (both Life Technologies).

Time-lapse microscopy was performed on an inverted Axio Observer (Carl Zeiss, Jena, Germany) equipped with an automated stage, a DG4 light source (Sutter Instrument, Novato, CA) for epifluorescence illumination, a VIS-LED for phase contrast imaging, and a CoolSnap-HQ2 camera (Photometrics, Tucson, AZ), driven by VisiView software (Visitron Systems, Puchheim, Germany). For some

experiments, an inverted microscope (Axiovert 100 TV; Carl Zeiss) was used, equipped with an HXP 120 lamp for epifluorescence illumination, a halogen lamp for phase-contrast imaging, and a CoolSnap-HQ2 camera, as well as electronic shutters driven by MetaMorph software (Molecular Devices, Sunnyvale, CA) for image acquisition. Verification of protein expression of EGFP or mCherry-tagged overexpression constructs was done using standard epifluorescence imaging.

Determination of rates of lamellipodium protrusion

Lamellipodium protrusion at 2 d posttransfection was determined based on kymographs generated from time-lapse movies as follows: lamellipodia of B16-F1 cells were recorded over at least 5 min, acquiring images every 15 s. Kymographs were generated using MetaMorph software by manually drawing lines from inside the cell and across the lamellipodium. Corresponding regions from each time point of a time-lapse series were pasted next to each other along the *x*-axis. Protrusion rates were determined by measuring advance of lamellipodia tips (*y*-axis) over time (*x*-axis). Time-lapse images for generation of kymographs for protrusion assays were obtained with 63×/1.4 NA Apochromat or 63×/1.25 NA Neofluor Plan oil objectives. Average values of lamellipodial protrusion rates, as shown in Figure 1C, are represented as percentage of the average protrusion rate of control EGFP-C1 blank vector–overexpressing cells, which were measured in parallel and used as a reference for each experiment.

Determination of rates of lamellipodial width and actin network polymerization

Actin assembly rate is defined as the sum of actin retrograde flow and protrusion of the corresponding lamellipodium tip for a given time period. Actin assembly rates in lamellipodia of B16-F1 cells were determined after co-overexpression of various EGFP- or mCherry-tagged constructs as indicated with either mCherry-Lifeact or EGFP-Lifeact coexpression, respectively. Distances traveled by fluorescence inhomogeneities within the actin meshwork over time were measured as cells protruded, allowing for calculation of lamellipodial actin polymerization rates. Live-cell images in these experiments were acquired using 100×/1.4 NA Plan apochromatic or 100×/1.3 NA Plan Neofluar oil objectives.

Width of respective lamellipodia was measured in cells co-overexpressing various EGFP- or mCherry-tagged constructs as indicated, again with the respective other fluorescent marker tagged to Lifeact, allowing for visualization of the lamellipodial actin meshwork. Lines crossing the width of lamellipodia from its tip to lamella were manually drawn for each cell and measured in MetaMorph software.

Photoactivation of fluorescently tagged actin

For photoactivation of actin, B16-F1 cells were cotransfected with human β-actin tagged to PA-GFP (Patterson and Lippincott-Schwartz, 2002) and either mRuby-Lifeact (for Figure 5; not shown in Figure 5B) or mCherry-tagged versions of either VASP full-length or mDia1-FH1-FH2 (for Figure 6 and Supplemental Figures S3 and S4). FRAP experiments were carried out essentially as described (Steffen *et al.*, 2014) on an inverted Axio Observer equipped with DG4 light source (Sutter Instrument) for epifluorescence illumination, a CoolSnap-HQ2 camera driven by VisiView software (2.1.0), and a photomanipulation device (Visitron Systems). PA-GFP-actin was photoactivated in selected regions with the 2D-VisiFRAP Realtime Scanner, using ~3- to 15-mW output power of an acousto-optical tunable filter–controlled 405-nm diode laser (settings: 10-pixel laser beam diameter, 1 ms FRAP time/pixel), estimated to give an activation time of between 300 and 600 ms. Activation was routinely initiated by manual trigger immediately during image acquisition. Frame rates were 0.33 Hz for the time-lapse recordings shown in Figure 5 and 0.75 Hz in all other experiments. Red/green dual-channel imaging was performed in the experiment in Figure 5 (red channel not shown in Figure 5B) and PA-GFP-actin imaging alone in all other experiments. Expression of mCherry-tagged VASP full-length or mDia1-FH1-FH2 was confirmed by individual images before and after time-lapse recordings for each cell. Images were acquired with a 100×/1.4 NA Plan apochromatic oil immersion objective, except for images in Figure 5, which were done with a 63×/1.4 NA Plan-Apochromat objective.

To analyze the reduction of cytosolically photoactivated actin within photoactivated regions over time, a region encompassing the photoactivated cytosolic region was manually drawn on MetaMorph software, and fluorescence intensities in this region were recorded for each frame. GFP-actin intensities over time were expressed as average percentage of the intensity of the same region at time 0 of photoactivation, which corresponded to 100% for each cell.

To analyze the incorporation of cytosolically photoactivated actin into lamellipodia, average pixel intensities in two separate regions were measured: 1) the cytosolically photoactivated region and 2) a lamellipodial region of ~1 µm width and 10 µm length constantly repositioned on the leading edge of lamellipodia during protrusion. Incorporation of photoactivated GFP-actin over time in the lamellipodium was expressed as percentage of the intensity of the cytosolic activation region at time 0 of photoactivation. For each cell, both lamellipodial fluorescence intensities and those of cytosolically photoactivated regions were normalized to their respective intensity values at the last frame before photoactivation.

Analysis of cytosolic dispersion of photoactivated actin was performed as follows: average pixel intensities were determined for the cytosolic activation region and a panel of regions each measuring 13.15 μm^2 in area and consecutively positioned distally from the activation region, collectively encompassing an average distance of ~10.5–11 µm in length (Supplemental Figure S3). Photoactivatable actin incorporation in each of the three regions for each time point is expressed as percentage of the intensity of the photoactivated region at time 0 of photoactivation.

All average intensities were corrected for background regions outside of the cell measured with MetaMorph 7.8.10 and processed with Microsoft Excel 2010 (Microsoft, Redmond, WA).

Quantification of total actin protein levels in EGFP-tagged constructs by Western blotting

Protein lysates for Western blots (shown in Supplemental Figure S5) were prepared as follows: B16-F1 cells were transfected overnight with the respective EGFP-tagged constructs or EGFP-C1 vector as control. Nontransfected cells were eliminated by incubation for 24 h in B16-F1 cell culture medium containing 2.5 µg/ml puromycin (Sigma-Aldrich). At 24 h later, cells were washed three times with ice-cold PBS and lysed with lysis buffer containing 50 mM Tris, pH 7.5, 150 mM NaCl, 1 mM EDTA, 1% Triton X-100, and Complete mini EDTA-free Protease Inhibitor Cocktail (Roche). Lysates were mixed thoroughly and protein amounts quantified (without prior centrifuging) using the Pierce BCA Protein Assay Kit (Thermo Fisher Scientific). Protein amounts were adjusted to 30 µg for each sample before addition of 8× SDS loading buffer in a 1:1 volume ratio. Samples were syringed several times through a

27-gauge needle and boiled for 10 min at 95°C. Western blotting was done according to standard procedures and using the following primary antibodies and concentrations: 1:10,000 mouse monoclonal anti–glyceraldehyde-3-phosphate dehydrogenase (GAPDH; 6C5; Calbiochem, Merck Millipore, Germany) and 1:1,000 mouse monoclonal anti-actin (clone AC-40, A3853; Sigma-Aldrich). Proteins from 10% acrylamide gels were transferred onto polyvinylidene fluoride (PVDF) membranes and exposed using Intas ECL Chemical imager (Intas Science Imaging, Göttingen, Germany). Intensity quantifications of protein bands of exposed membranes were performed on ImageJ v1.46r. Identical rectangular regions were drawn around protein bands of interests, and actin protein amounts were normalized to external background and respective GAPDH controls.

Immunoprecipitations

Ectopically expressed EGFP-tagged FMNL2-FH2 (Supplemental Figure S2) was immunoprecipitated using GFP-Trap_A (ChromoTek). After overnight transient transfection, confluent B16-F1 cells were lysed using IP buffer (140 mM KCl, 50 mM Tris-HCl, pH 7.4, 50 mM NaF, 10 mM $Na_4P_2O_7$, 2 mM $MgCl_2$, 1% Triton X-100, and a Mini Complete Protease Inhibitor Pill [Roche]). Lysates were centrifuged at 20,000 × *g* for 15 min at 4°C and mixed with SDS sample buffer. Bead slurry was washed with IP buffer lacking Triton X-100 and centrifuged at 2500 × *g* for 2 min at 4°C. Cell lysates were then added to the beads and incubated under constant mixing for 1 h at 4°C. After another centrifugation (2,500 × *g*, 2 min, 4°C), supernatants were incubated with sample buffer and defined as control for unbound, EGFP-tagged proteins. Beads were washed with IP before addition of SDS sample buffer. All samples were boiled at 95°C for 5 min and proteins blotted onto PVDF membranes (Immobilon). Anti-actin antibody (clone AC-40, A3853; Sigma-Aldrich) was used to confirm coimmunoprecipitation of actin with EGFP-tagged bait. Ponceau S stain for general protein staining of membranes was purchased from Sigma-Aldrich.

Data processing and statistical analyses

Brightness and contrast levels were adjusted using MetaMorph software v7.7.8.0. Images were further processed for figure preparation using Adobe Photoshop CS4 (Adobe Systems, San Jose, CA). Line scans in Supplemental Figure S1 were generated using the line scan function in MetaMorph software v7.7.8.0. Final figures were assembled with Photoshop CS4 or Adobe Illustrator CS4 (Adobe Systems). Data analyses were carried out in ImageJ and MetaMorph, Microsoft Excel 2010, and Sigma plot 12.0 (Systat Software, Erkrath, Germany). Data sets were compared using Mann–Whitney rank sum test or Spearman rank order correlation test (Sigma plot 12.0). Probability of error of 5% or less ($*p < 0.05$) was considered statistically significant.

ACKNOWLEDGMENTS

We thank Roland Wedlich-Söldner for DNA constructs, T. E. Stradal (Helmholtz Centre for Infection Research, Braunschweig, Germany) and J. Faix (Hannover Medical School, Hannover, Germany) for discussion, and Gerd Landsberg and Brigitte Denker for excellent technical assistance. This work was supported in part by Deutsche Forschungsgemeinschaft Grants RO2414/3-2 and RO2414/5-1 to K.R. and Seventh Framework Programme Grant FORCEFULACTIN of the European Research Council to M.F.C. and K.R.

REFERENCES

Bear JE, Loureiro JJ, Libova I, Fassler R, Wehland J, Gertler FB (2000). Negative regulation of fibroblast motility by Ena/VASP proteins. Cell 101, 717–728.

Block J, Breitsprecher D, Kuhn S, Winterhoff M, Kage F, Geffers R, Duwe P, Rohn JL, Baum B, Brakebusch C, *et al*. (2012). FMNL2 drives actin-based protrusion and migration downstream of Cdc42. Curr Biol 22, 1005–1012.

Campellone KG, Welch MD (2010). A nucleator arms race: cellular control of actin assembly. Nat Rev Mol Cell Biol 11, 237–251.

Carl UD, Pollmann M, Orr E, Gertlere FB, Chakraborty T, Wehland J (1999). Aromatic and basic residues within the EVH1 domain of VASP specify its interaction with proline-rich ligands. Curr Biol 9, 715–718.

Cramer LP (1999). Role of actin-filament disassembly in lamellipodium protrusion in motile cells revealed using the drug jasplakinolide. Curr Biol 9, 1095–1105.

Fakhri N, Wessel AD, Willms C, Pasquali M, Klopfenstein DR, MacKintosh FC, Schmidt CF (2014). High-resolution mapping of intracellular fluctuations using carbon nanotubes. Science 344, 1031–1035.

Harris ES, Gauvin TJ, Heimsath EG, Higgs HN (2010). Assembly of filopodia by the formin FRL2 (FMNL3). Cytoskeleton 67, 755–772.

Harris ES, Rouiller I, Hanein D, Higgs HN (2006). Mechanistic differences in actin bundling activity of two mammalian formins, FRL1 and mDia2. J Biol Chem 281, 14383–14392.

Innocenti M, Zucconi A, Disanza A, Frittoli E, Areces LB, Steffen A, Stradal TE, Di Fiore PP, Carlier MF, Scita G (2004). Abi1 is essential for the formation and activation of a WAVE2 signalling complex. Nat Cell Biol 6, 319–327.

Isogai T, van der Kammen R, Leyton-Puig D, Kedziora KM, Jalink K, Innocenti M (2015). Initiation of lamellipodia and ruffles involves cooperation between mDia1 and the Arp2/3 complex. J Cell Sci 128, 3796–3810.

Iwasa JH, Mullins RD (2007). Spatial and temporal relationships between actin-filament nucleation, capping, and disassembly. Curr Biol 17, 395–406.

Kage F, Winterhoff M, Dimchev V, Mueller J, Thalheim T, Freise A, Bruhmann S, Kollasser J, Block J, Dimchev GA, *et al*. (2017). FMNL formins boost lamellipodial force generation. Nat Commun 8, 14832.

Koestler SA, Auinger S, Vinzenz M, Rottner K, Small JV (2008). Differentially oriented populations of actin filaments generated in lamellipodia collaborate in pushing and pausing at the cell front. Nat Cell Biol 10, 306–313.

Koestler SA, Rottner K, Lai F, Block J, Vinzenz M, Small JV (2009). F- and G-actin concentrations in lamellipodia of moving cells. PLoS One 4, e4810.

Koestler SA, Steffen A, Nemethova M, Winterhoff M, Luo N, Holleboom JM, Krupp J, Jacob S, Vinzenz M, Schur F, *et al*. (2013). Arp2/3 complex is essential for actin network treadmilling as well as for targeting of capping protein and cofilin. Mol Biol Cell 24, 2861–2875.

Krause M, Gautreau A (2014). Steering cell migration: lamellipodium dynamics and the regulation of directional persistence. Nat Rev Mol Cell Biol 15, 577–590.

Lai FP, Szczodrak M, Block J, Faix J, Breitsprecher D, Mannherz HG, Stradal TE, Dunn GA, Small JV, Rottner K (2008). Arp2/3 complex interactions and actin network turnover in lamellipodia. EMBO J 27, 982–992.

Machesky LM, Insall RH (1998). Scar1 and the related Wiskott-Aldrich syndrome protein, WASP, regulate the actin cytoskeleton through the Arp2/3 complex. Curr Biol 8, 1347–1356.

McGrath JL, Tardy Y, Dewey CF Jr, Meister JJ, Hartwig JH (1998). Simultaneous measurements of actin filament turnover, filament fraction, and monomer diffusion in endothelial cells. Biophys J 75, 2070–2078.

Millard TH, Behrendt B, Launay S, Futterer K, Machesky LM (2003). Identification and characterisation of a novel human isoform of Arp2/3 complex subunit p16-ARC/ARPC5. Cell Motil Cytoskeleton 54, 81–90.

Miyoshi T, Tsuji T, Higashida C, Hertzog M, Fujita A, Narumiya S, Scita G, Watanabe N (2006). Actin turnover-dependent fast dissociation of capping protein in the dendritic nucleation actin network: evidence of frequent filament severing. J Cell Biol 175, 947–955.

Mullins RD, Heuser JA, Pollard TD (1998). The interaction of Arp2/3 complex with actin: nucleation, high affinity pointed end capping, and formation of branching networks of filaments. Proc Natl Acad Sci USA 95, 6181–6186.

Olazabal IM, Caron E, May RC, Schilling K, Knecht DA, Machesky LM (2002). Rho-kinase and myosin-II control phagocytic cup formation during CR, but not FcgammaR, phagocytosis. Curr Biol 12, 1413–1418.

Patterson GH, Lippincott-Schwartz J (2002). A photoactivatable GFP for selective photolabeling of proteins and cells. Science 297, 1873–1877.

Peckham M, Miller G, Wells C, Zicha D, Dunn GA (2001). Specific changes to the mechanism of cell locomotion induced by overexpression of beta-actin. J Cell Sci 114, 1367–1377.
Pernier J, Shekhar S, Jegou A, Guichard B, Carlier MF (2016). Profilin interaction with actin filament barbed end controls dynamic instability, capping, branching, and motility. Dev Cell 36, 201–214.
Pollard TD, Borisy GG (2003). Cellular motility driven by assembly and disassembly of actin filaments. Cell 112, 453–465.
Rajakyla EK, Vartiainen MK (2014). Rho, nuclear actin, and actin-binding proteins in the regulation of transcription and gene expression. Small GTPases 5, e27539.
Ridley AJ (2011). Life at the leading edge. Cell 145, 1012–1022.
Riedl J, Crevenna AH, Kessenbrock K, Yu JH, Neukirchen D, Bista M, Bradke F, Jenne D, Holak TA, Werb Z, *et al*. (2008). Lifeact: a versatile marker to visualize F-actin. Nat Methods 5, 605–607.
Rottner K, Behrendt B, Small JV, Wehland J (1999). VASP dynamics during lamellipodia protrusion. Nat Cell Biol 1, 321–322.
Rotty JD, Wu C, Haynes EM, Suarez C, Winkelman JD, Johnson HE, Haugh JM, Kovar DR, Bear JE (2015). Profilin-1 serves as a gatekeeper for actin assembly by Arp2/3-dependent and -independent pathways. Dev Cell 32, 54–67.
Samarin S, Romero S, Kocks C, Didry D, Pantaloni D, Carlier MF (2003). How VASP enhances actin-based motility. J Cell Biol 163, 131–142.
Small JV, Stradal T, Vignal E, Rottner K (2002). The lamellipodium: where motility begins. Trends Cell Biol 12, 112–120.
Steffen A, Koestler SA, Rottner K (2014). Requirements for and consequences of Rac-dependent protrusion. Eur J Cell Biol 93, 184–193.
Steffen A, Ladwein M, Dimchev GA, Hein A, Schwenkmezger L, Arens S, Ladwein KI, Margit Holleboom J, Schur F, Victor Small J, *et al*. (2013). Rac function is crucial for cell migration but is not required for spreading and focal adhesion formation. J Cell Sci Suppl 126, 4572–4588.
Steffen A, Rottner K, Ehinger J, Innocenti M, Scita G, Wehland J, Stradal TE (2004). Sra-1 and Nap1 link Rac to actin assembly driving lamellipodia formation. EMBO J 23, 749–759.
Suarez C, Carroll RT, Burke TA, Christensen JR, Bestul AJ, Sees JA, James ML, Sirotkin V, Kovar DR (2015). Profilin regulates F-actin network homeostasis by favoring formin over Arp2/3 complex. Dev Cell 32, 43–53.
Suraneni P, Rubinstein B, Unruh JR, Durnin M, Hanein D, Li R (2012). The Arp2/3 complex is required for lamellipodia extension and directional fibroblast cell migration. J Cell Biol 197, 239–251.
Svitkina TM, Bulanova EA, Chaga OY, Vignjevic DM, Kojima S, Vasiliev JM, Borisy GG (2003). Mechanism of filopodia initiation by reorganization of a dendritic network. J Cell Biol 160, 409–421.
Vitriol EA, McMillen LM, Kapustina M, Gomez SM, Vavylonis D, Zheng JQ (2015). Two functionally distinct sources of actin monomers supply the leading edge of lamellipodia. Cell Rep 11, 433–445.
Vitriol EA, Wise AL, Berginski ME, Bamburg JR, Zheng JQ (2013). Instantaneous inactivation of cofilin reveals its function of F-actin disassembly in lamellipodia. Mol Biol Cell 24, 2238–2247.
Wang YL (1985). Exchange of actin subunits at the leading edge of living fibroblasts: possible role of treadmilling. J Cell Biol 101, 597–602.
Watanabe N, Mitchison TJ (2002). Single-molecule speckle analysis of actin filament turnover in lamellipodia. Science 295, 1083–1086.
Wu C, Asokan SB, Berginski ME, Haynes EM, Sharpless NE, Griffith JD, Gomez SM, Bear JE (2012). Arp2/3 is critical for lamellipodia and response to extracellular matrix cues but is dispensable for chemotaxis. Cell 148, 973–987.
Yang C, Czech L, Gerboth S, Kojima S, Scita G, Svitkina T (2007). Novel roles of formin mDia2 in lamellipodia and filopodia formation in motile cells. PLoS Biol 5, e317.
Zicha D, Dobbie IM, Holt MR, Monypenny J, Soong DY, Gray C, Dunn GA (2003). Rapid actin transport during cell protrusion. Science 300, 142–145.